FEM STUDY OF A SYNCHRONOUS MOTOR WITH DIFFERENT PERMANENT MAGNET TOPOLOGIES

Ovidiu CRAIU[1], Teodor Ionuț ICHIM[2], Liviu POPESCU[3]

The paper presents a study of a Permanent Magnet Synchronous Motor (PMSM) with 10 poles and 12 slots having different permanent magnet configurations. Bread loaf surface mounted magnets, radially embedded in the rotor, internal magnets, or Halbach magnets distribution were modeled with the professional software COMSOL Multiphysics. The influence of the different motor topologies upon the shape of the motor phase and line-to-line back EMF and load voltages, as well as on the torque ripple and cogging torque amplitude is analyzed. The Finite Element Method (FEM) quasi-stationary models were coupled with the stator circuit equations to simulate the sinusoidal current supply of the motor. The results are mainly qualitative, the purpose is to assist in motor design strategy and show some of the complexity of the choices in such a process.

Keywords: permanent magnet synchronous motor, finite element method, back electromotive force, electromagnetic torque

1. Introduction

This paper presents the analysis of a PMSM motor, fed with alternative sinusoidal currents. The PMSM runs smoother than a Brushless DC motor (BLDC), with less torque ripple, and can operate within a larger speed span than BLDC, by using flux weakening [1].

The same motor can be used either as BLDC or as PMSM, designing and choosing this type of motor is done according to refined, but important factors. Among these, the most important is the ratio between the number of pole pairs and slots, according to which the stator winding can be a lap or a tooth (concentrating) winding, and the shape, position, and magnetization direction of the permanent magnets. According to these factors, the motor back EMF and airgap magnetic field distribution become more sinusoidal or closer to a trapezoidal shape, making the motor more suitable to operate as PMSM or as BLDC, respectively.

[1] Faculty of Electrical Engineering, University POLITEHNICA Bucharest, Romania, E-mail: ocraiu@yahoo.com
[2] ICPE S.A. – Messico, Romania, E-mail: ichim_teodor@yahoo.com
[3] Faculty of Electrical Engineering, University POLITEHNICA Bucharest, Romania, E-mail: liviu_p@yahoo.com

As analyzing all factors (winding type and magnet shape, magnetization, and position) at the same time would be too complex, in this paper a brushless permanent motor with 10 poles and 12 slots was considered. That is a typical slot-pole combination used in PMSM motors generating a short-pitched, slot winding. It has the advantage of short end-turns and compact construction specific to tooth windings and has a close to one winding factor for the fundamental frequency (short-pitching, in this case, does not reduce much the linkage flux and thus the torque). Although more suitable for PMSM by reducing harmonics and producing a more sinusoidal field distribution in the airgap, the tooth windings advantages (and specifically the 10 poles –12 slots much-used combination), make them used also in BLDC machines [2-4].

With this slot-pole combination fixed, various permanent magnet topologies were analyzed, using FEM numerical models. The sinusoidal currents in the stator were considered by coupling stator circuit equations to FEM magnetic field models and the shape of the phase and line-to-line back EMF, and terminal voltage, as well as torque vs rotor position dependences, were analyzed.

To allow a consistent comparison, the stator lamination geometry was maintained unchanged (or changed slightly), as well as motor length, maximum voltage, and slot ampere-turns. Smaller deviations were made in some of the models to achieve the best torque out of the motor and to maintain the same supply voltage at the same rotor speed.

The requirements, such as flat/constant torque and EMF for a BLDC or a sinusoidal torque and EMF for a PMSM and a small torque ripple in both cases, are achieved through different techniques concerning the magnet shape, the direction of the magnetization, placement on either the surface or embedded inside the rotor, the type of winding, number of poles, pole pitch, etc. All these factors equal many design choices and explain the versatility and diversity of the PM brushless machines [3,5].

To determine the right number of turns per coil, the load terminal voltage had to be as close as possible to the supply peak value. Apart from using all available voltage, opting for a higher number of turns would allow the motor to operate at a smaller current and obtain the same torque while reducing Joule losses and enhancing motor efficiency [8].

2. Numerical model

The FEM 2D time-variable electromagnetic field models were coupled with the stator electric circuit equations. Using the “Rotating Machinery, Magnet” module of COMSOL Multiphysics software it was possible to connect the rotor moving mesh with the stator fix mesh without reconstructing the geometry and the

mesh [6]. The magnetic field produced by the three-phase stator current rotates synchronously with the rotor magnetic field.

There are no eddy currents considered as in the rotor the magnetic field is constant and in the stator the gauge of the copper used for windings is small. Based on magnetic vector potential **A**, the formulation takes into account magnetic nonlinearity:

$$\nabla\times\left(\frac{1}{\mu}\nabla\times\mathbf{A}\right)=\mathbf{J}+\nabla\times\left(\frac{1}{\mu}\mathbf{B}_r\right) \tag{1}$$

with **J** current density. The current density results from the electric circuit equations coupled with FEM field equations. Motor permanent magnets are modeled considering a linear demagnetization characteristic defined by remanent induction $\mathbf{B}_r$ and equivalent magnetic permeability μ. While the curl of a constant $\mathbf{B}_r$ cancels inside permanent magnet domains, on the permanent magnet boundaries the curl is non-zero and contributes to equation (1).

The electromagnetic torque was computed using Arkkio's relation, which is a Maxwellian tensor pondered on a surface but is also equivalent to the virtual work method, and thus is more precise than the tensor's method [7,8].

$$T=\frac{l_i}{\mu_0(r_e-r_i)}\int_S rB_rB_\phi\,\mathrm{d}S \tag{2}$$

with **S** the section in the air-gap area comprised between the inner radius r_i and outer radius r_e, B_r and B_φ being the radial and tangential magnetic flux densities.

Fig. 1 Stator circuit.

The stator circuit shown in Fig. 1 was modeled and connected to FEM field equations. The two sinusoidal current sources I_1 and I_2 are given by:

$$\begin{aligned} I_1 &= I_{\max}\sin(\omega t+\varphi)\\ I_2 &= I_{\max}\sin(\omega t+\varphi-2\pi/3)\text{'} \end{aligned} \tag{3}$$

have the same current amplitude $I_{\max}$, pulsation $\omega = p \times \Omega$, with $p = 5$ the number of pole pairs and Ω the constant rotor angular velocity. The phase angle φ is chosen in such a way to produce the maximum torque i.e., the magnetic field produced by the permanent magnets and the stator armature reaction being in quadrature. The current in the third phase results to meet the condition that the sum of the currents is always nil in node 11. The resistors R1, R2, and R3 represent the resistance of the coils, computed by default in COMSOL if the coil module is used to define each phase. Coil electric resistivity was increased to

account for the contribution of the end turns to the phase resistance. L1, L2, and L3 are the end turn impedances, which are small and can be neglected. E1, E2, and E3 are representing the back EMF produced by the phase coils. The no-load EMF is computed by making zero the source currents in the circuit.

3. Numerical results

Numerical results were obtained for a PMSM with ten poles and twelve slots. The study contains different topologies of permanent magnets with different shapes and placed on the rotor or in the interior of the rotor, parallel or radial magnetized, with Halbach distribution or without, and made of SmCo32 with remnant flux density B_r = 1.1T and relative magnetic permeability μ_r = 1.03. The stator laminations are made of silicon steel 50PN250. The winding is concentrated with coils wound around the teeth; the number of turns depends on the EMF which must not exceed the voltage supplied. This slot-pole combination is useful also in DC brushless machines.

To achieve a more consistent comparison between different constructive versions, the following data was kept unchanged for all studied motor versions: the number of slots and number of poles; the supply current: all motors are supplied with a sinusoidal current of equal amplitude and frequency and phase angle chosen to produce maximum torque; the stator outer diameter; the motor axial length.

The best solution for this study was used to produce a motor prototype. Due to contractual limitations, some of the geometrical data, the number of turns per coil (slightly different from model to model), as well as the current maximum values, are not going to be disclosed. The main purpose is to present various constructive shapes and different ways of embedding permanent magnets into a PMSM rotor. A brief qualitative comparison among solutions is presented further. Using field-circuit FEM models, it was possible to compute the no-load voltage (motor back EMF), as well as the phase and line-to-line voltages at maximum load/current. To determine the right number of turns, the terminal voltage at full load must not exceed, but be close to the supply peak voltage.

3.1. Bread-loaf magnets

The first PMSM model has bread-loaf-shaped magnets. This magnet shape is more suitable for PMSM than for BLDC motors, as it produces a more sinusoidal field distribution in the airgap [9,10]. The airgap under the magnet is uneven, smaller in the middle, and larger at the sides. The greater the difference between magnet and airgap radii, the more sinusoidal the magnetic flux becomes. Due to physical symmetry, the model consists of one-half of motor geometry, Fig. 2.

By modifying the magnet width and magnet top radius, it was possible to optimize the torque-time variation. As shown in Fig. 3, the torque ripple is rather reduced (the torque axis was magnified for better visualization of torque oscillations). Cogging torque has twice the frequency of the torque ripple, which means at load, torque oscillation is created not only by reluctance but also by magnetic saturation [11].

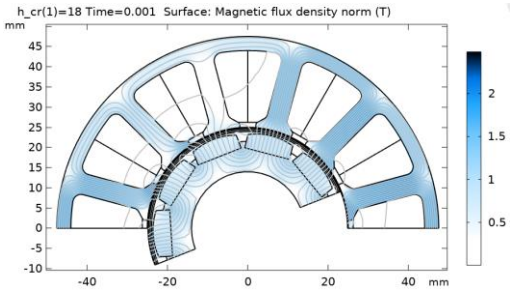

Fig. 2 Magnetic flux distribution for a motor with bread loaf magnets.

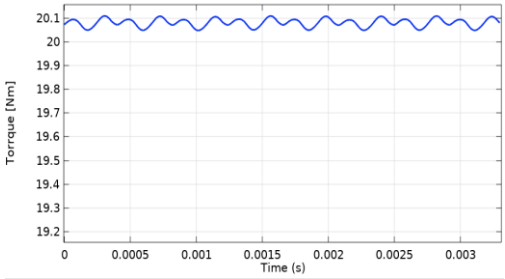

Fig. 3 The torque-time variation.

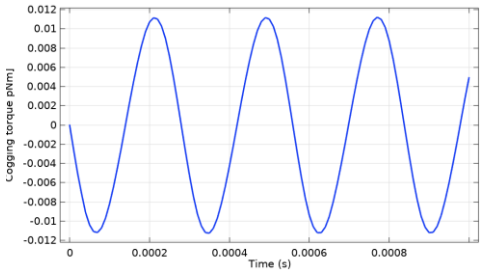

Fig. 4 Cogging torque for the bread-loaf magnet shape.

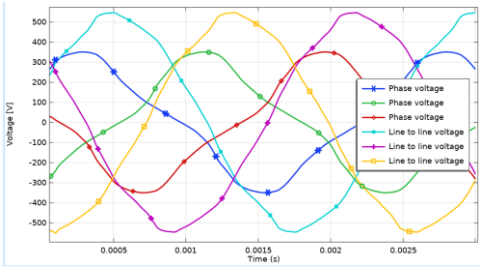

Fig. 5 Line to line and phase voltages for a higher speed.

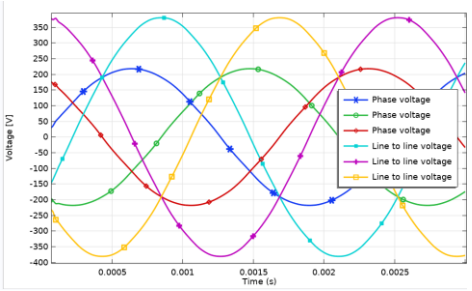

Fig. 6 Line to line and phase EMS, at no-load computed at the highest speed.

As in non-salient synchronous motors, the motor electromagnetic torque is proportional to the product between no-load EMF and current in the armature coil, the right conclusion was that smoothening the torque in the motor can be achieved by analyzing and optimizing the no-load EMF shape in such a way to obtain a waveform as sinusoidal as possible. However, in the presence of saliency, specific to PMSM, especially in motors with interior permanent magnets the best optimization would be based on torque-time analysis instead of EMF shape, as cogging increases torque ripple. As phase windings are wye connected, multiple three-order harmonics vanish from the line-to-line voltage (Fig. 5, solid and dot

lines) which is why it has a more sinusoidal shape than phase voltage time-variation (Fig. 5, dashed line). The no-load EMF waveform, Fig. 6, is close to a sinewave, thereby the resulting torque has a reduced ripple.

3.2. Radially embedded magnets

In Fig. 7 is presented the magnetic flux distribution in half of the PMSM with radial embedded magnets (spoke-type magnets) [12,13]. Such structure is usually used for ferrites to increase airgap magnetic flux. However, for this model same SmCo magnets were used as before. The rotor yoke is very narrow to prevent magnetic flux from closing from one magnet to the next through the yoke and to push it towards the airgap.

Compared to the previous solution, the magnet volume was increased obtaining almost the same torque with a reduced number of turns per coil, thus with less copper, or, at the same slot filling factor, with an increased conductor section. On the other hand, to make room for the magnets, the inner rotor diameter was significantly reduced compared to the previous solution, increasing the rotor mass and moment of inertia.

Given the reduced magnetic permeability of the rare earth magnets (close to that of air), thicker PM means an increased magnetic circuit equivalent reluctance. That translates to a lower operational point of the permanent magnets, which is a less efficient usage of the magnet energy.

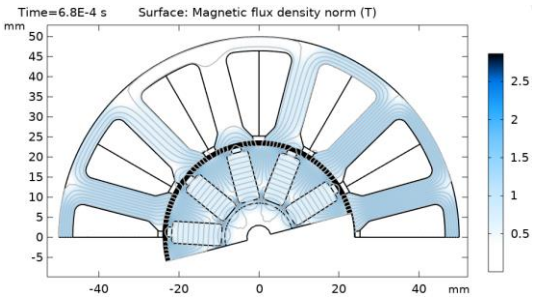

Fig. 7 Magnetic flux distribution for radially placed PM.

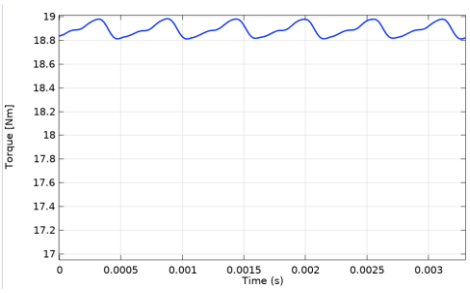

Fig. 8 Torque-time variation.

Torque ripple is higher than in the previous version, Fig. 8, as the motor has more saliency than the previous model. That is also noticed in the shape of the back EMF waveform, which is slightly less sinusoidal than in the previous model, Fig. 11. Due to magnetic saturation and variable reluctance, the line-to-line voltage is less sinusoidal than in the previous model, Fig. 9. Torque was obtained at the same rated current, but the number of turns per coil was slightly reduced so that peak terminal voltage does not exceed its maximum value.

Cogging torque is reduced, Fig. 10, due to reduced slot openings in the stator and rotor, which is an advantage of this model.

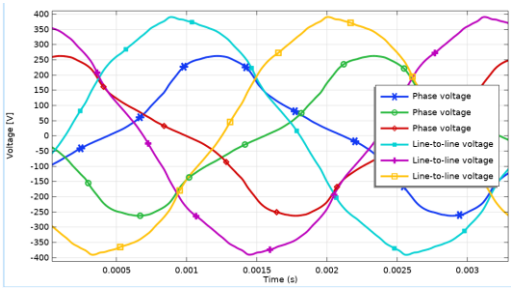

Fig. 9 Line-to-line voltage, and phase voltage for radially placed PM.

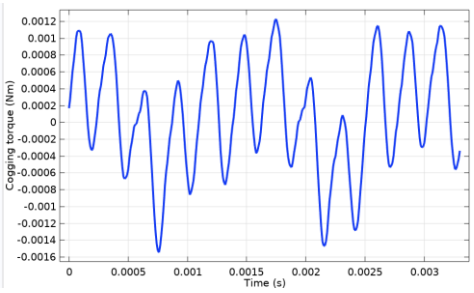

Fig. 10 Cogging torque is significantly smaller than the previous model

3.3. Radially embedded magnets with partial Halbach area

A similar construction with radially distributed permanent magnets is presented in Fig. 11. The difference is made by the smaller magnets with perpendicular magnetization, added between the main radially distributed magnets, forming a hybrid Halbach area distribution. This kind of solution was analyzed from the perspective of reducing the permanent magnet volume.

Compared to the previous solution, the torque is reduced, decreasing from 19 Nm to 15 Nm, Fig. 12. Due to higher magnetic saliency and larger slot openings in the rotor, the torque ripple increased. Similarly, cogging torque represented in Fig. 14 becomes larger than in the previous model, making this solution less desirable. At load, the phase voltage variation is less sinusoidal, Fig. 13, but the line-to-line voltage waveform remains rather sinusoidal. The phase voltage and line-to-line voltage are comparable to the ones used in the previous model, Fig. 9, as the same number of turns per coil was used, and they were computed at the same maximum rotor speed. This shows that with reduced magnet volume, the motor produces less torque; in comparison, this motor has a lower power density than the previous model.

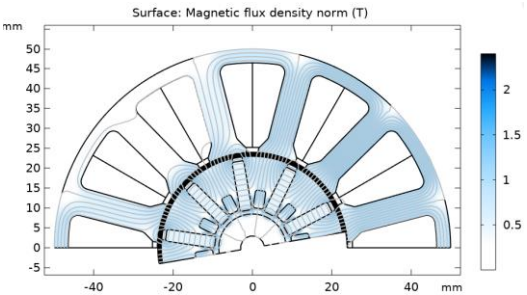

Fig. 11 Magnetic flux distribution for embedded PM with partial Halbach area distribution.

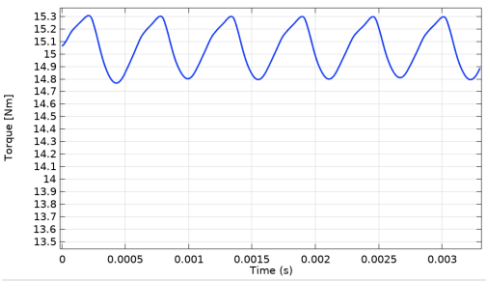

Fig. 12 The variation of torque ripple, at 15 Nm torque.

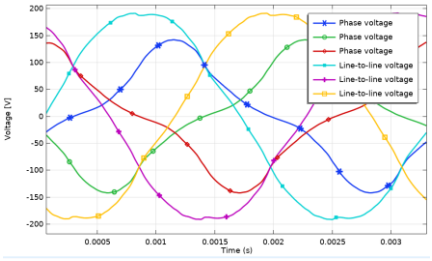

Fig. 13 Line-to-line and phase voltages.

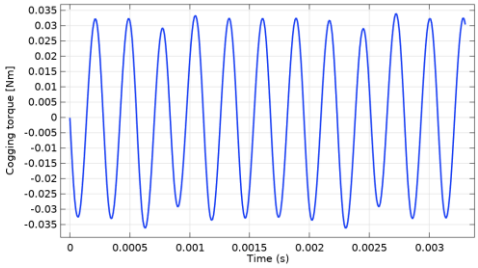

Fig. 14 Cogging torque variation.

3.4. Interior Permanent magnet (IPM) configuration

This is a different rotor configuration with stator geometry kept unchanged for an easier and more relevant comparison, Fig. 15. This solution is more difficult to produce, as rotor perforations can be achieved only if the rotor is made of laminations. A construction that prevents the magnetic short-circuit between consecutive permanent magnets is in general difficult to achieve for any IPM PMSM topology. Instead, the motor will have a reduced equivalent airgap and a higher magnetic flux density in the airgap as a result [14,15]. As in any IPM configuration, the PM should not be too thick, as that would decrease magnetic circuit equivalent permeance, which will, in turn, reduce magnetic induction in the PM operational point.

A similar analysis as in the previous motor configurations was performed. The torque ripple, Fig. 16 appeared to be larger than in the previous cases, while maximum torque kept a similar value as in the previous case, but smaller than in the first model. This is due to the fact the IPM configurations are more sensitive to magnetic circuit geometrical optimization.

More work should be done to obtain a circuit with a reduced leakage flux. Indeed, magnet volume cannot be too high in this case. In contrast, permanent magnets can be easily inserted in their rotor locations, and thus do not require mechanical reinforcement such as cans or gluing. That is an advantage as it reduces manufacturing costs and allows for a reduced motor airgap.

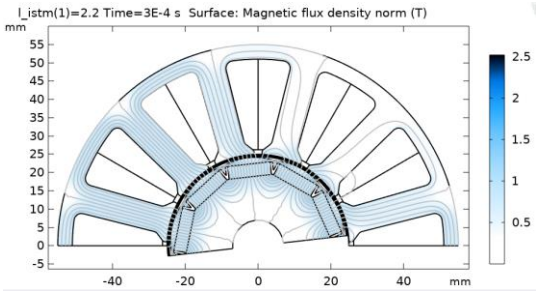

Fig. 15 Flux distribution and magnetic flux lines for the IPM construction.

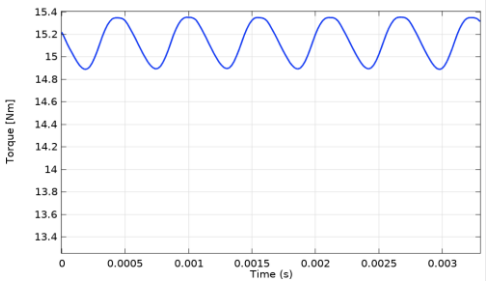

Fig. 16 Torque variation for PMSM with IPM topology.

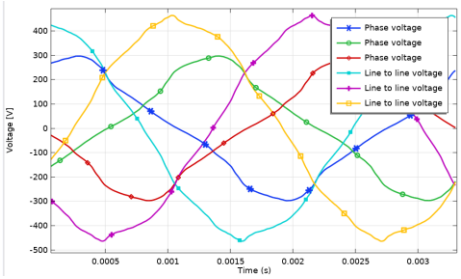

Fig. 17 Line-to-line voltage and phase voltage for the IPM construction.

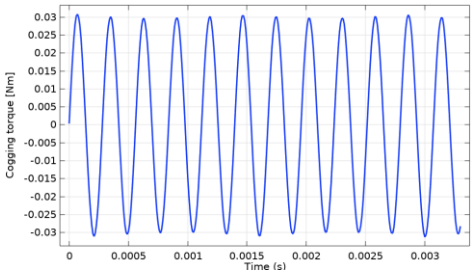

Fig. 18 The cogging torque.

Voltage waveforms at load are rather deformed, Fig. 17, but are closer to a sinewave at no-load (not plotted), which is necessary for a smooth operation with a lower torque ripple.

The cogging torque is not too high and has similar values as in the previous model, Fig. 18. This solution has the advantages of a reduced magnet volume and higher saliency which is good when applying the flux weakening technique to increase the motor speed.

3.5. No-gap surface-mounted magnets

In Fig. 20 is presented the geometry of a PMSM with no-gap surface-mounted magnets. This is a solution chosen for optimizing the space occupied by magnets so that a maximum volume of magnets can be used. As an increased magnetic flux produced by the rotor passes through the stator, small changes to the stator lamination geometry had to be made compared to the previous models, to avoid teeth and yoke magnetic saturation. As in the previous models, the same rare earth permanent magnets with equal remanent flux density, relative permeability, and parallelly magnetized, were used.

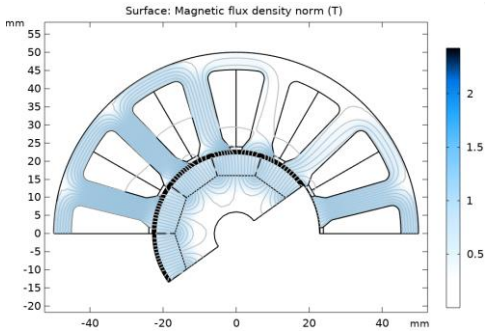

Fig. 20 The flux distribution and magnetic field lines for no-gap surface-mounted magnets.

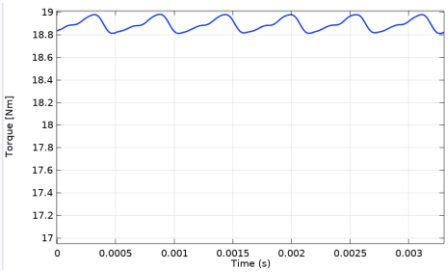

Fig. 21 The variation of torque ripple at 19 Nm torque.

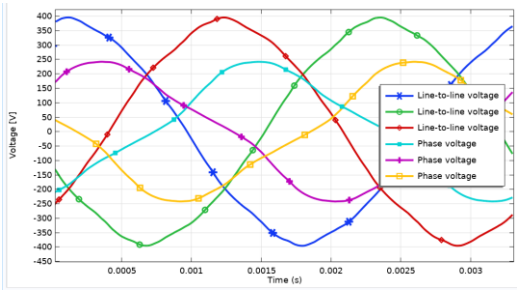

Fig. 22 Line-to-line and phase voltages for a no-gap surface mounted magnet.

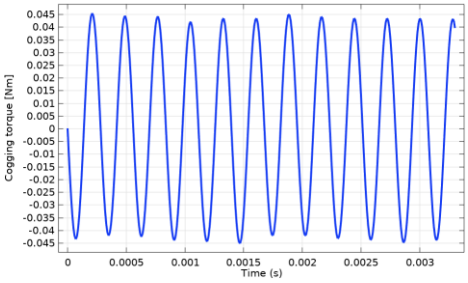

Fig. 23 The cogging torque.

Compared to the previous two solutions, this configuration produced, as expected, higher torque and almost half of the ripple, Fig. 21. Different than the IPM configuration, this motor requires a sleeve (can) over the magnets to prevent centrifugal force to dislocate them from the rotor. That can be a slight disadvantage as the rotor sleeve will add to the total airgap length. This configuration permits a reduction of the rotor yoke and the rotor inertia when the motor shaft is hollow. The voltage variation at load operation is closer to a sinewave, Fig. 22, and even more so is the line-to-line back EMF. Because of the EMF sinusoidal shape, at no load (not plotted) the motor has a reduced ripple. To that also contributes the motor's low magnetic saturation obtained by optimizing stator lamination geometry, as well as the very reduced rotor saliency (due to its polygonal shape, close to a circle). The maximum torque is larger than in the previous solutions with some noticeable percentage, although the current and the peak supplied voltage were kept unchanged.

Cogging torque is within the limits of the other models, Fig. 23.

This is the motor with the highest power density of all models, apart from the last topology with Halbach distribution. Given its simple rotor geometry (with no need for special perforations as in the IMP configuration), and no eddy currents in the rotor, the rotor can be made of solid magnetic steel. Polygonal rotor faces are easy to manufacture and will assist in mounting the magnets in their position. The rotor's inner diameter can be diminished and that reduces the rotor mass and inertia.

3.6. V-shape inner mounted magnets

This is a configuration that can be used to increase the volume of magnets and ensure some saliency of the motor. Saliency is useful in PMSM to assist in vector field control and, in applying field weakening to increase the speed.

As in the previous IPM solutions, the rotor must be laminated, so that rotor perforations and the room for embedding the magnets are easier to make, Fig. 24. With the stator kept unchanged from the previous models, this configuration proved to have a higher power density and offers the advantage of an easy mount

of the magnets, without the need for gluing them. In contrast, the torque ripple has higher values than in other constructive solutions, Fig. 25, due to motor variable reluctance. Cogging torque has also an elevated value, Fig. 27, if compared to the previous solutions.

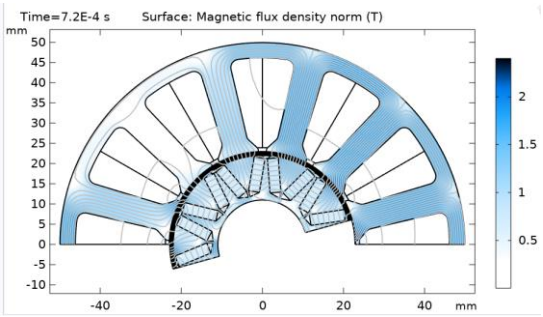

Fig. 24 Magnetic field lines and flux distribution for PMSM with V-shaped magnets.

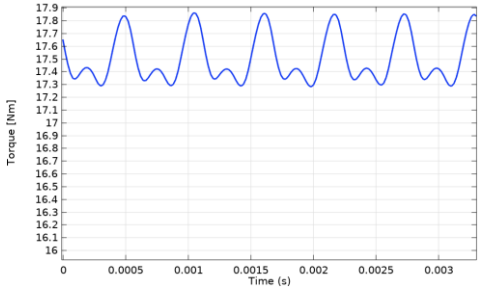

Fig. 25 The variation of torque ripple for V-shaped IPM configuration.

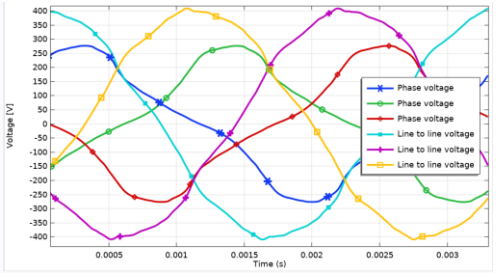

Fig. 26 Line-to-line and phase back EMF, at load.

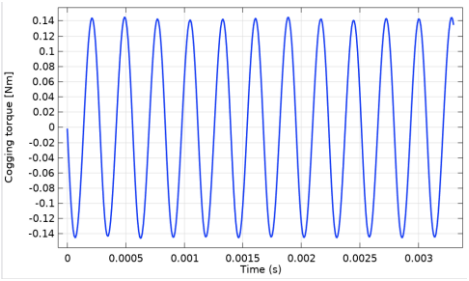

Fig. 27 The representation of cogging torque.

The line-to-line and phase voltages are presented in fig. 26 and are less sinusoidal.

3.7. Halbach area configuration and perforated stator teeth

This is a constructive solution that uses a Halbach area permanent magnet distribution and is the topology with the highest power density [16]. Due to magnet distribution, the rotor back iron can be small [17], the field being strong on the airgap side of the magnet Halbach area and weak towards the shaft. Thus, the rotor hollow can be enlarged, which allows reducing rotor mass and its moment of inertia, Fig. 28.

The stator geometry was optimized to allow the passage of a higher magnetic flux – i.e., larger stator yoke and teeth width. The slot openings were increased to reduce torque ripple. That is also helping for easier insertion of the winding coils inside the slots. In addition, the teeth were provided with a semicircular perforation which permitted a controlled magnetic saturation of the teeth that flattened the torque time-variation curve.

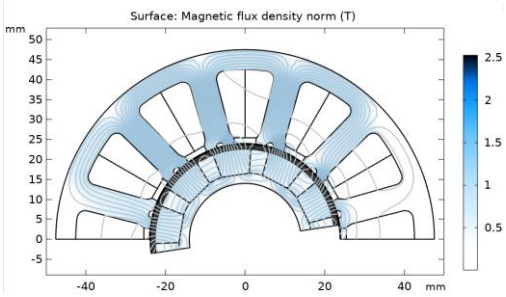

Fig. 28 Magnetic flux density and streamlines for the motor with Halbach area configuration.

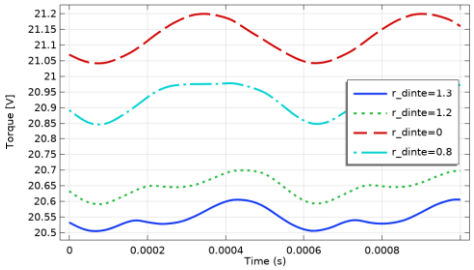

Fig. 29 Torque-time variation for different perforation radii.

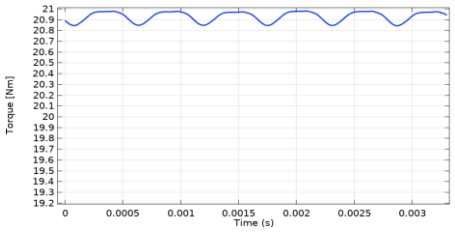

Fig. 30 The representation of ripple torque at a maximum current.

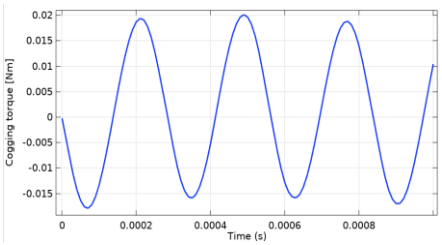

Fig. 31 Cogging torque time variation.

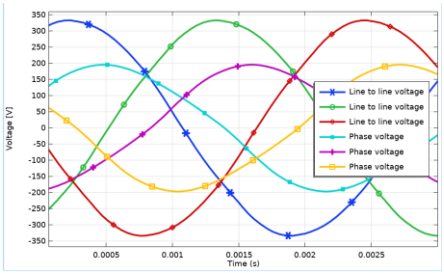

Fig. 32 Line-to-line and phase voltages at highest speed at load.

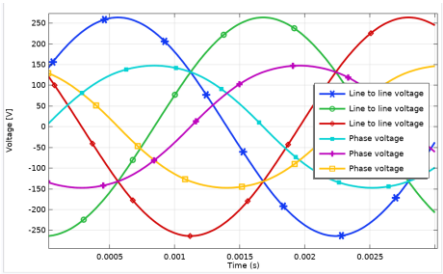

Fig. 33 Line-to-line and phase voltages at no-load.

The dashed curve in Fig. 29 shows the torque time-variation for the motor with no tooth perforation. The bottom curve (solid line Fig.29) corresponds to the largest tooth perforation; the plotted torque-time dependency does not have the smallest ripple, and because of the perforation its average torque was diminished. A compromise solution was adopted (the dot-dashed line Fig. 29) which corresponds to an average-sized tooth perforation for which ripple is the smallest while the average torque is not too reduced.

The cogging torque, Fig. 31, is also smaller than the cogging of the motor with bread loaf magnets, Fig. 2. That is a confirmation that permanent magnets with a Halbach area produce in general a sinusoidal distribution of the magnetic field at the airgap level. The only other configuration that had a lower torque ripple than the current topology, was the motor with bread loaf magnets.

The voltage waveforms at load operation are the closest to a sinusoidal form, Fig. 32. Due to the absence of space between magnets, having a smooth circular rotor surface, the motor has no saliency, hence the low ripple and small cogging torque. The back EMF determined at no-load is also very close to sinusoidal, Fig. 33.

4. Conclusions

The magnets' shape and their position on/within the rotor make important differences in motor operation. Various motor topologies generate different shapes of the no-load back EMF waveforms, torque ripple, and cogging torque. Since a more sinusoidal no-load EMF would be better for a PMSM, optimization based on analyzing the back EMF time variation is often adopted for obtaining a better motor with smoother operation and less noise. A more trapezoidal EMF waveform shape would be more convenient for a BLDC and could be also a good criterion for optimization in that case. Higher saliency would be beneficial for PMSM, for vector field control or flux weakening, and can be easier obtained with embedded magnets in the rotor. However, as shown in this study, higher saliency also has the disadvantage of producing a higher torque ripple, even in the case of sinusoidal like EMF. On the other hand, motors with low saliency used mainly in BLDC, such as those with surfaced mounted PM, proved to be feasible also for PMSM solutions.

An increase of torque or speed even with few percentages, or reducing cogging torque and ripple, can be important aspects in designing a motor [18-20].

The results and graphics presented should be considered qualitative and are provided as a guide for designing such a PMSM. Numerical results, the back EMF, or torque time variations can be easily verified by experimental testing and are a confirmation of the quality of the built motor.

R E F E R E N C E S

[1]. *Cristina Soviany*, Embedding Data and Task Parallelism in Image Processing Applications, Ph.D. Thesis, Technische Universiteit Delft, 2003

[1]. *J.R. Hendershot, T.J.E. Miller*, Design of Brushless Permanent-Magnet Machines, Motor Design Books LLC; Second Edition, 2010.

[2]. *N. Bianchi, S. Bolognani, M.D. Pre, G. Grezzani*, Design considerations for fractional-slot winding configurations of synchronous machines, IEEE Transactions on Industry Applications, Vol. 42, No. 4, p.997-1006, 2006.

[3]. *Varaticeanu, Bogdan & Minciunescu, Paul & Nicolescu,* C. Performance comparison between surface, spoke and interior permanent magnet machines designed for traction applications. Revue Roumaine des Sciences Techniques Serie Electrotechnique et Energetique, 2016, 61. 3-7.

[4]. *J. Cros and P. Viarouge*, Synthesis of High-Performance PM Motors With Concentrated Windings, IEEE Transactions On Energy Conversion, Vol. 17, no. 2, June 2002.

[5]. *M. Modreanu, Mircea & Andrei, Mihail-Iulian & Morega, Mihaela & Tiberiu, Tudorache.* Brushless DC micro-motor with surface mounted permanent magnets. Revue Roumaine des Sciences Techniques - Serie Électrotechnique et Énergétique. 2014, 59. 237-247.
[6]. COMSOL Multiphysics, v 5.3, Reference Manual, User's Guide, Copyright© 1998-2018.
[7]. *Arkkio,* Analysis of Induction Motors Based on the Numerical Solution of the Magnetic Field and Circuit Equations, Ph.D. Thesis, Helsinki 1987, UDC 621.313.33: 519.62/.64.
[8]. *N. Sadowski, Y. Lefevre, M. Lajoie-Mazenc, J. Cros,* Finite Element Torque Calculation in Electrical Machines while Considering Movement, IEEE Trans. On MAG, vol. 28, No.2, March 1992, p. 1410-1413.
[9]. *A.M. El-Refaie, T.M. Jahns, D.W. Novotny,* Analysis of surface PM machines with fractional-slot concentrated windings, IEEE Trans. on Energy Conv, Vol. 21, No. 1, p. 34-43, 2006.
[10]. *P. P. Ling, Dahaman Ishak, T. L. Tiang,* Influence of magnet pole arc variation on the performance of external rotor permanent magnet synchronous machine based on finite element analysis, 2016 IEEE International Conference on Power and Energy (PECon).
[11]. *M. Lajoie-Mazenc, J. M. Vinassa, J. Cros, and S. Astier,* Brushless dc motors with low torque ripple, in Proc. Stockholm Power Tech. Conf., Stockholm, Sweden, June 18–22, 1995, pp. 87–92.
[12]. *W. Zhao, T. A. Lipo and B. Kwon,* Torque pulsation minimization in spoke-type interior permanent magnet motors with skewing and sinusoidal permanent magnet configurations, IEEE Trans. Magn., vol. 51, no. 11, Nov. 2015.
[13]. *P. Zhang, G. Y. Sizov, D. M. Ionel, and N. A. O. Demerdash,* Establishing the relative merits of interior and spoke-type permanent magnet machines with ferrite or NdFeB through systematic design optimization, IEEE Transactions on Industry Applications, vol. 51, no. 4, pp. 2940–2948, July 2015.
[14]. *J. Liang, A. Parsapour, Z. Yang, C.s Caicedo-Narvaez, M. Moallem, B. Fahimi,* Optimization of Air-Gap Profile in Interior Permanent-Magnet Synchronous Motors for Torque Ripple Mitigation, IEEE Transactions on Transportation Electrification, Vol. 5, No. 1, March 2019.
[15]. *S.M. Sue, K. L. Wu, J. S. Syu and K. C. Lee,* A Phase Advanced Commutation Scheme for IPM-BLDC Motor Drives, in Proc. of the IEEE-ICIEA 2209, pp.2010-2013, May 2009.
[16]. *H. A. Khazdozian, R. L. Hadimani, D. Jiles,* Size Reduction of Permanent Magnet Generators for Wind Turbines Using Halbach Cylinders, 2015 IEEE International Magnetics Conference (INTERMAG), 2015.
[17]. *R. P. Praveen, M. H. Ravichandran, V. T. Sadasivan Achari, V. P. Jagathy Raj, G. Madhu, and G. R. Bindu,* A Novel Slotless Halbach-Array Permanent-Magnet Brushless DC Motor for Spacecraft Applications, IEEE Transactions on Industrial Electronics, Vol. 59, No. 9, p. 3553-3559, September 2012.
[18]. *P. Renaud, S. Louis, P. Damien, and A. Miraoui*, Design optimization method of BLDC motors within an industrial context, 2017 IEEE International Electric Machines and Drives Conference (IEMDC), 2017, pp. 1-7.
[19]. *Z. Zhang and L. Zhou,* Electromagnetic performance analysis of multilayer interior PMSM with fractional slot concentrated windings for electric vehicle applications, Turkish Journal of Electrical Engineering and Computer Sciences, vol. 23, no. 6, pp. 1638–1644, 2015.
[20]. *O. Craiu, L. Melcescu, C. Boboc, M. Modreanu,* Proiectarea asistată a unui servomotor de curent continuu cu magneți permanenți cu caracteristica de cuplu și dimensiuni impuse, Simpozionul de Mașini Electrice SME'15 – 23 Octombrie, 2015.